

## ACICULAR SPHALERITE ENRICHED IN Ag, Sb, AND Cu EMBEDDED WITHIN COLOR-BANDED SPHALERITE FROM THE KOKANEE RANGE, BRITISH COLUMBIA, CANADA

GEORGES BEAUDOIN<sup>§</sup>

*Département de géologie et de génie géologique, Université Laval, Québec, Québec G1K 7P4, Canada*

### ABSTRACT

Sphalerite from the Kokanee Range, British Columbia, displays color banding ranging from light to dark brown. Sphalerite forms massive layers with a dark base enriched in Fe and Cu. Layers have sharp boundaries that can be planar or undulating. The base of the sphalerite layers commonly contains acicular crystals of sphalerite oriented perpendicular to the layer boundary. Acicular sphalerite is enriched in Sb, Ag and Cu, which substitute for Zn in the structure. The base of the layers is commonly marked by chains of complex inclusions of chalcopyrite, galena, pyrrargyrite and freibergite, which mimic color banding. The layer thickness displays a lognormal distribution ascribed to a random process; it is interpreted to be dependent on the amount of hydrothermal fluid introduced within a fracture prior to precipitation of a layer. The acicular sphalerite probably inverted from rapidly precipitated wurtzite formed from a solution enriched in Cu, Fe, Ag and Sb, an inference that is supported by chains of sulfides and sulfosalts at the base of ferroan sphalerite layers. The precipitation of acicular wurtzite would have depleted the solution in Cu, Ag, Sb, the acicular crystals becoming embedded in Zn-rich sphalerite. Under those conditions, the color banding of sphalerite is controlled by local conditions, which prevents its use for correlation (sphalerite stratigraphy) from one vein to the other.

*Keywords:* silver, antimony, copper, zinc, sphalerite, vein, layer, acicular, crystal, Kokanee Range, British Columbia.

### SOMMAIRE

La sphalérite de la chaîne de Kokanee, en Colombie-Britannique, présente des bandes de couleurs brun pâle à foncé. La sphalérite forme des couches massives avec une base foncée enrichie en Cu et en Fe. Les couches ont des limites abruptes qui peuvent être planaires ou ondulantes. La sphalérite aciculaire est enrichie en Sb, Ag et Cu, qui remplacent le Zn dans la structure. La base des couches de sphalérite est généralement le site de chaînes d'inclusions de chalcopyrite, galène, pyrrargyrite et freibergite, qui miment les bandes de couleurs. L'épaisseur des bandes de sphalérite présente une distribution log-normale qui pourrait causer un processus aléatoire dépendant de la quantité de fluide hydrothermal injecté dans une fracture avant la précipitation d'une couche de sphalérite. La sphalérite aciculaire serait un produit de l'inversion de la wurtzite métastable, précipitée rapidement à partir d'une solution enrichie en Cu, Fe, Ag et Sb, ce qui est aussi indiqué par les inclusions de sulfures et sulfosels à la base des couches de sphalérite. La précipitation de la wurtzite aciculaire aurait appauvri la solution en Cu, Ag et Sb, de sorte que celle-ci deviendrait enrobée de sphalérite riche en Zn. Sous ces conditions, les bandes de couleur dans la sphalérite seraient le produit de processus locaux qui empêchent son usage pour la corrélation d'une veine à l'autre grâce à la stratigraphie de la sphalérite.

*Mots-clés:* argent, antimoine, cuivre, zinc, sphalérite, veine, bande, aciculaire, cristal, chaîne de Kokanee, Colombie-Britannique.

### INTRODUCTION

Sphalerite (ZnS) displays a wide range of colors in nature. These result from the incorporation of several elements, most notably Fe, in the structure. In addition, natural sphalerite may display bands of various colors, most commonly in various types of silver – lead – zinc and gold–silver epithermal veins and in Mississippi-Valley-type deposits (Barton & Bethke 1987). This color banding has been used to define time lines within

the paragenetic sequence of mineralization, and is commonly referred to as “sphalerite stratigraphy” (*e.g.*, McLimans *et al.* 1980). A detailed description of the sphalerite bands and of the internal texture of the color bands is rarely provided, however. One has the impression of regular, planar layers of sphalerite of varying color. Yet in some cases the internal structure of the color bands has been shown to be complex, comprising subparallel internal bands and oriented rows of sulfide inclusions (Patrick *et al.* 1993). The internal texture of

<sup>§</sup> *E-mail address:* beaudoin@ggl.ulaval.ca

the color bands, indeed, should be documented to obtain important information on chemical and physical processes active during precipitation of sulfide minerals from hydrothermal solutions.

Silver–lead–zinc veins in the Kokanee Range, southeastern British Columbia (Fig. 1), contain sphalerite that commonly displays megascopic color-banding (Beaudoin 1991). The unmetamorphosed veins formed during Eocene crustal extension (Beaudoin *et al.* 1992a). The veins are in fractures and faults zones, or form replacement bodies of massive sulfide adjacent to the veins. More than 370 deposits have recorded production, thus forming a vein field that was infiltrated by the same hydrothermal fluids (Beaudoin *et al.* 1992b). The mineralogy is dominated by massive galena and sphalerite with accessory pyrite, pyrrothite, chalcopyrite, argentite, freibergite, pyrrargyrite and a diverse suite of silver and sulfosalt minerals. The gangue is comprised of massive siderite or quartz with minor dolomite, late calcite and rare fluorite and barite. The veins are surrounded by narrow halos of phyllic alteration. Attempts to establish a “sphalerite stratigraphy” were unsuccessful because the color banding is complex and discontinuous and cannot be correlated between deposits. Detailed examination of the color-banded sphalerite, however, revealed complex and unusual textures within the banded sphalerite that are described below.

#### COMPOSITION AND STRUCTURE OF THE SPHALERITE

Sphalerite can incorporate a diverse suite of chemical elements in its structure. Fe, Cd, and Cu commonly substitute for Zn in sphalerite, whereas Pb, In, Ga, Ge, Hg, Sn, and Mn occur more sporadically (Barton *et al.* 1977, Burke & Kieft 1980, McLimans *et al.* 1980, Oen *et al.* 1980, Möller 1985, Johan 1988, Patrick *et al.* 1993, Dini *et al.* 1995, Kuhlemann & Zeeh 1995, Ueno *et al.* 1996). The hydrothermal experiments of Kogima & Sugaki (1985) indicate that up to 1.2 wt.% Cu is soluble in sphalerite. Several other investigators used bulk analytical methods on sphalerite concentrates, which may explain the diverse suite of elements reported (Ag, As, Ba, Co, Hg, Mo, Ni, Sb, and Tl; Warren & Thompson 1945, Ramdohr 1969, Viets *et al.* 1992, Kuhlemann & Zeeh 1995). Experimental studies have not been done to evaluate the extent of incorporation of these elements in the sphalerite structure.

Ueno *et al.* (1996) reviewed the conditions under which the hexagonal polymorph wurtzite inverts to sphalerite. Hydrothermal experiments indicates that wurtzite formation is favored by rapid precipitation from highly supersaturated hydrothermal solutions (Kojima & Ohmoto 1991). Also, wurtzite is favored in hydrothermal systems characterized by a low fugacity of sulfur (Scott & Barnes 1972). The review of Ueno *et al.* (1996) shows that incorporation of trace elements such as Mn, Cd and Fe decreases significantly the inversion temperature of wurtzite to sphalerite.

#### SPHALERITE TEXTURES

The sphalerite crystals display megascopic color-banding (Fig. 2) ranging from light to dark brown. Doubly polished thin sections allow observation of thinner bands and of fine textures within color bands that are not visible in standard polished thin sections. There is no expression of the color-banding under incident illumination. Megascopic color-banding results from two dominant textures: alternating layers of darker and lighter sphalerite (Fig. 3A), and acicular aggregates of sphalerite (Fig. 3B).

#### Layered sphalerite

Layered crystals of sphalerite grew from the margin toward the center of the vein. The vein selvage is covered by several crystals through which color layers are continuous (Fig. 2). Coprecipitated quartz also displays growth zonation caused by abundant fluid inclusions trapped during boiling of the hydrothermal fluid (Beaudoin *et al.* 1992b). Layers of light to dark brown sphalerite are commonly bound by sharp, planar, and parallel boundaries (Fig. 3C). Layered sphalerite outlines growth faces, as evidenced by sharp angles along parallel boundaries of the layers (Fig. 2). Layer thickness is commonly uniform over lateral distances of up to several mm. The color of sphalerite in one layer may display variations in tint. The most common is a dark brown base overlain by lighter brown top (Fig. 3A). The boundaries locally display small irregularities that depart from the planar form. Layer boundaries are locally not parallel, but the angle of departure from parallelism is commonly small (Fig. 3D). Sphalerite layers display

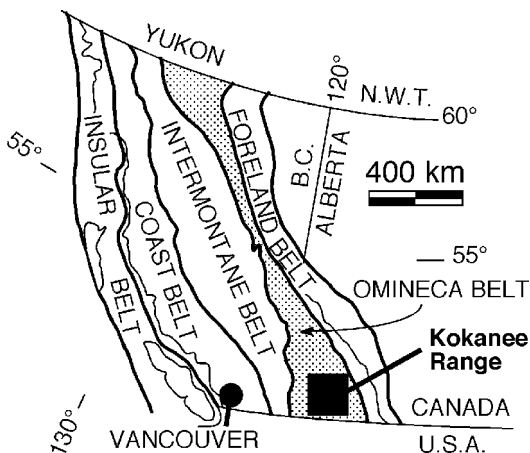


FIG. 1. Location of Kokanee Range in southeastern British Columbia.

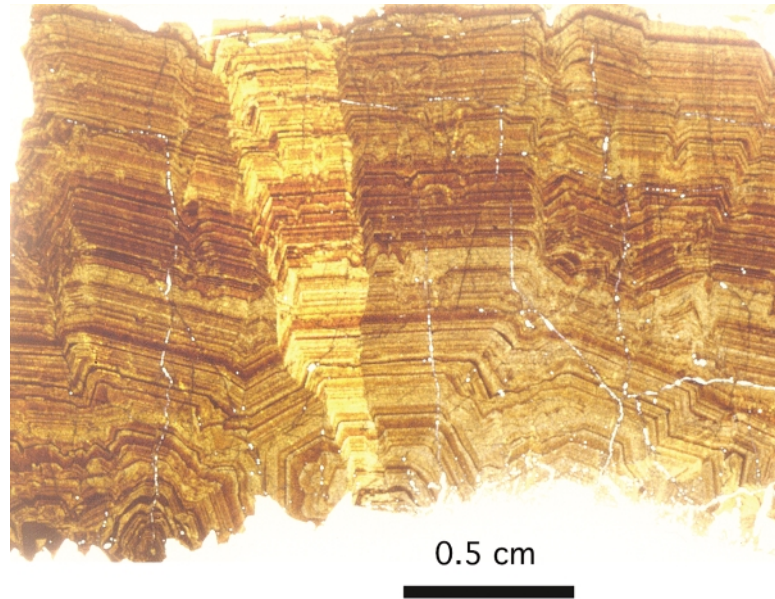


FIG. 2. Crystal displaying alternating bands of darker and lighter brown sphalerite with apparently random thicknesses and color. The crystal contains a large band dominated by darker sphalerite. Growth direction toward the top.

an internal texture that ranges from massive (Fig. 3C), to acicular crystals (Fig. 3B), to layers having complex internal textures comprised of several discontinuous sublayers at a small angle to the main layer (Fig. 3D). These internal sublayers resemble those described by Patrick *et al.* (1993), who used transmission electron microscopy to document rows of small inclusions of chalcopyrite in them. Exceptionally, layers have wavy boundaries (Fig. 3E). Layers may thicken and thin, and the color contrast may decrease laterally such that the layer seems to terminate. Evidence for sphalerite dissolution is provided by a later generation of sphalerite filling troughs cutting across layered sphalerite. In one location, the planar boundary between layers is disrupted, forming an irregular bump in the growth direction. The disruption is directly above a primary fluid inclusion within the dark brown sphalerite layer (Fig. 3F). This two-phase fluid–vapor inclusion yielded a temperature of homogenization of 238°C and a salinity of 12.8 wt.% NaCl eq. (Beaudoin *et al.* 1992b).

#### *Acicular sphalerite*

Acicular crystals of sphalerite occur within sphalerite layers. It is not possible to physically separate the acicular crystals from the matrix sphalerite. A representative sample comprising both layered and acicular sphalerite yielded an X-ray-diffraction pattern of

sphalerite only, such that there is no evidence that the acicular crystals are the hexagonal polymorph, wurtzite. The acicular crystals most commonly grew perpendicular from the base of a layer and are darker brown compared to the embedding massive sphalerite (Fig. 3B). The sphalerite needles are more closely packed near the growth base and become less dense and are well resolved optically in the growth direction (Fig. 4). The acicular crystals have a width of less than 1  $\mu\text{m}$  and a length of up to 120  $\mu\text{m}$ , with variable length within one layer. The close packing at the base of a layer seems to be a result of the occurrence of numerous shorter crystals (Fig. 4). The acicular crystals thin toward the tip, optically disappearing within the lighter brown matrix sphalerite (Fig. 3B). Acicular crystals commonly display a small range of orientations in one location (Fig. 5A).

In many layers, the color of the acicular crystals is dark brown and displays no significant variation in tint across layers of sphalerite with different tints (Fig. 3B). In other layers, however, there are variations in tint that are parallel to the layer boundaries (Fig. 5B). The darker base is overlain by lighter brown material, but the acicular crystals appear to be optically continuous across oscillatory color-zoned sphalerite (Fig. 5B). It is not always clear if the change in tint is from the massive matrix, from the acicular crystals themselves, or from variations in the density of acicular crystals near the base of a layer.

One spectacular texture displays a radiating aggregate of branching acicular crystals of dark brown sphalerite located in a trough formed by layered sphalerite (Fig. 5C). The radiating aggregate is embedded in a matrix of lighter brown, massive sphalerite. The acicular crystals display a branching texture characterized by

a major, linear branch joined by a large number of thin, short, and wavy branches at apparent angles close to  $30^\circ$  (Fig. 5D). The radiating aggregate is overlain and moulded by planar layers with sharp angles representing primary crystal-growth faces (Fig. 5C).

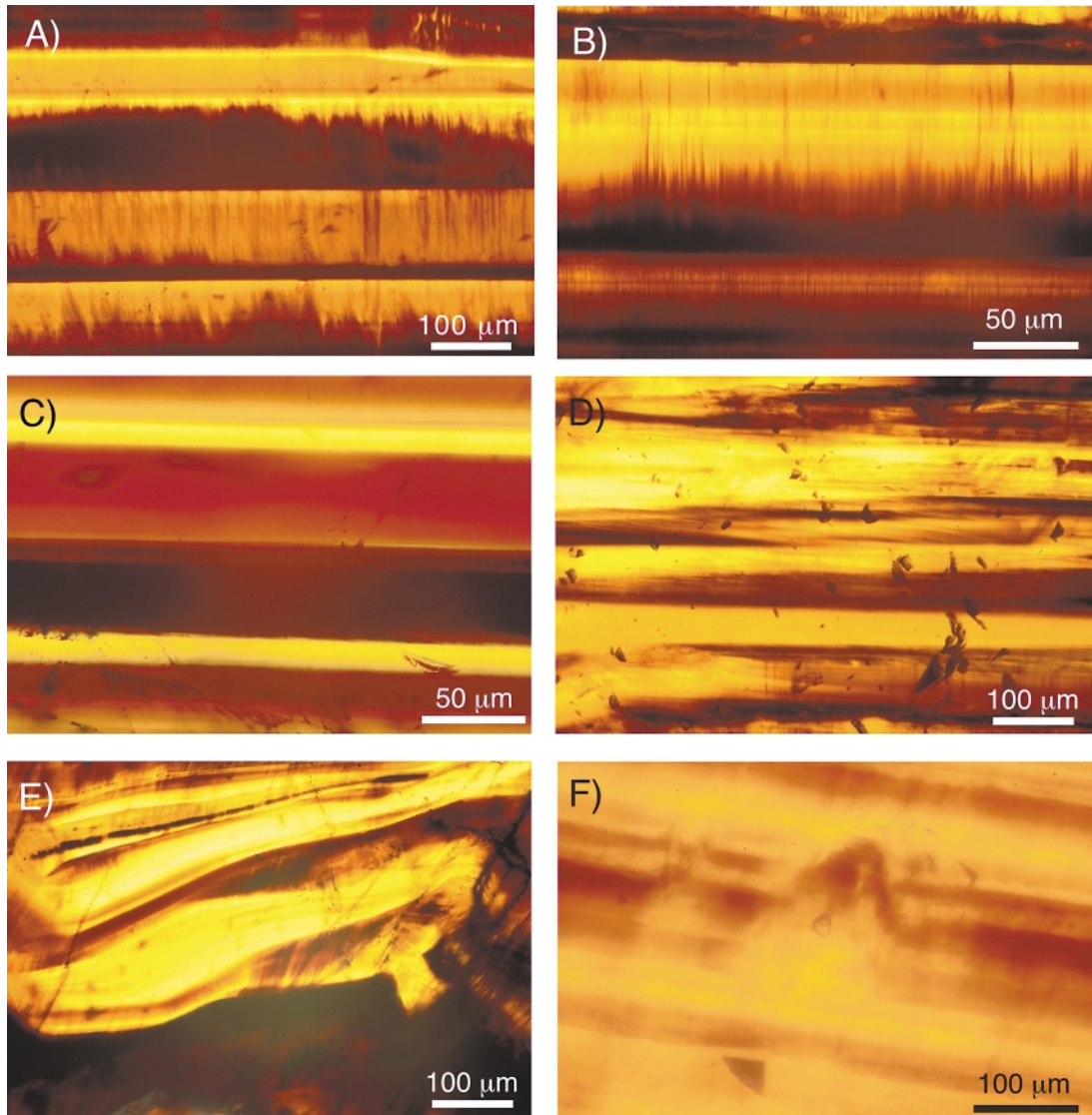


FIG. 3. A) Layered sphalerite with flat, parallel boundaries. Top of photo is in the growth direction. The layers display a dark base with a lighter upper part. Acicular crystals of sphalerite are approximately perpendicular to sphalerite layers. B) Acicular crystals of sphalerite of variable length embedded in a layered matrix of sphalerite. Acicular sphalerite crosses layered sphalerite or grows from the bottom of some layers. C) Parallel layers of massive sphalerite with flat boundaries. D) Subparallel layers with flat boundaries and internal oblique layering. E) Irregular, wispy layering. Some of the clear layers display an internal structure resembling the acicular crystals of sphalerite in Figure 3B). F) Liquid-vapor inclusion within layered sphalerite. The inclusion is overlain by disrupted layering in the direction of crystal growth.

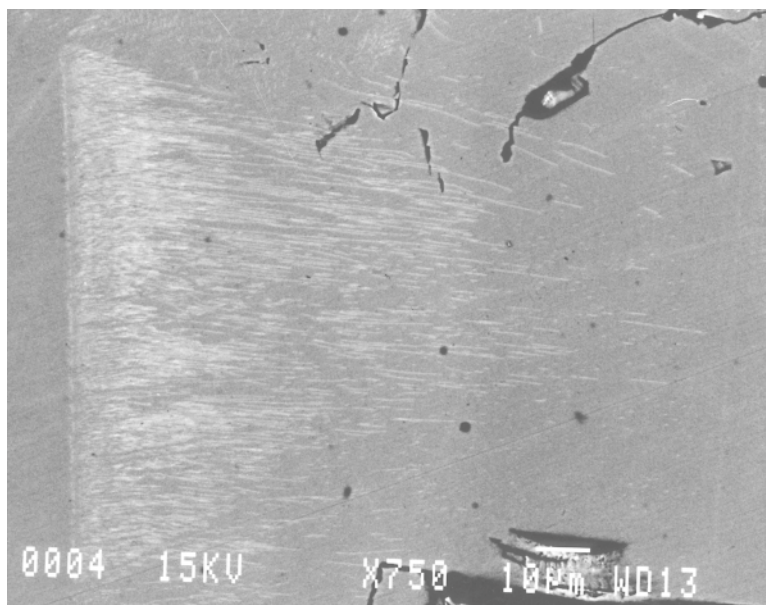


FIG. 4. SEM back-scattered electron image of acicular sphalerite crystals (light grey) with a higher mean Z number than the matrix of massive sphalerite (dark grey). Acicular sphalerite grows from the flat bottom boundary of the layer (vertical, left) and the density of acicular crystals decreases toward the top of the layer (right).

#### *Mineral inclusions in layered sphalerite*

The dark brown base of several layers is marked by chains of disseminated inclusions of sulfosalts and sulfides (Figs. 6A, B). The inclusions have round, elliptical, or irregular shapes, with a long dimension of less than 500  $\mu\text{m}$ . Larger inclusions are commonly complex, with intergrowths of chalcopyrite, galena, pyrrargyrite and freibergite (Fig. 6C). Some freibergite inclusions contain exsolved chalcopyrite that is elongate and oriented (Fig. 6D), whereas others are irregular to round and irregularly distributed.

#### CHEMICAL COMPOSITION OF SPHALERITE

##### *Analytical methods*

The chemical composition of the sphalerite was determined using the scanning electron microscope (SEM) for back-scattered electron imaging and the electron microprobe (EM) for point analysis and X-ray mapping. To study the complex and very fine texture of the sphalerite was an analytical challenge. Back-scattered electron mapping was performed at Université Laval using a JEOL 840 SEM, whereas point analyses and X-ray mapping were performed with electron microprobes (EM) at McGill University (JEOL-8900) and at the CAMECA factory in Paris (SX-100). Point analyses were performed with McGill University EM at 20 kV and

30 nA using natural sphalerite, chalcopyrite, pyrite and pure metal standards. The chemical variations were investigated at McGill University by wavelength-dispersion X-ray mapping over an area devoid of mineral inclusions measuring 1 mm  $\times$  1 mm at 20 kV and 30 nA using a dwell time of 50 ms over each of the 250 000 pixels measuring 2  $\mu\text{m}$   $\times$  2  $\mu\text{m}$ . To define more accurately the distribution of Zn, Fe, Ag, Sb, and Cu in areas where acicular sphalerite crystals are found, detailed X-ray mapping was performed using the SX-100. This mapping was done on a 50  $\times$  50  $\mu\text{m}$  area at 10 kV and 10 nA using a dwell time of 200 ms over each of the 262 144 pixels measuring each slightly less than 0.1  $\mu\text{m}$   $\times$  0.1  $\mu\text{m}$ . Under those conditions, the beam was estimated to have a diameter of 0.2  $\mu\text{m}$ , such that the signal acquired at each pixel represents an area three times larger than the size of the pixel. This is the maximum spatial resolution offered by the instrument at conditions optimized for the X-ray count rates. The effect of having a beam larger than the pixel size is to smooth compositional variations across adjacent pixels, but the beam diameter was narrower than the width of the acicular crystals.

##### *Results*

Back-scattered electron mapping of layered sphalerite shows subtle variations in the mean atomic mass, observable only under high-contrast analytical condi-

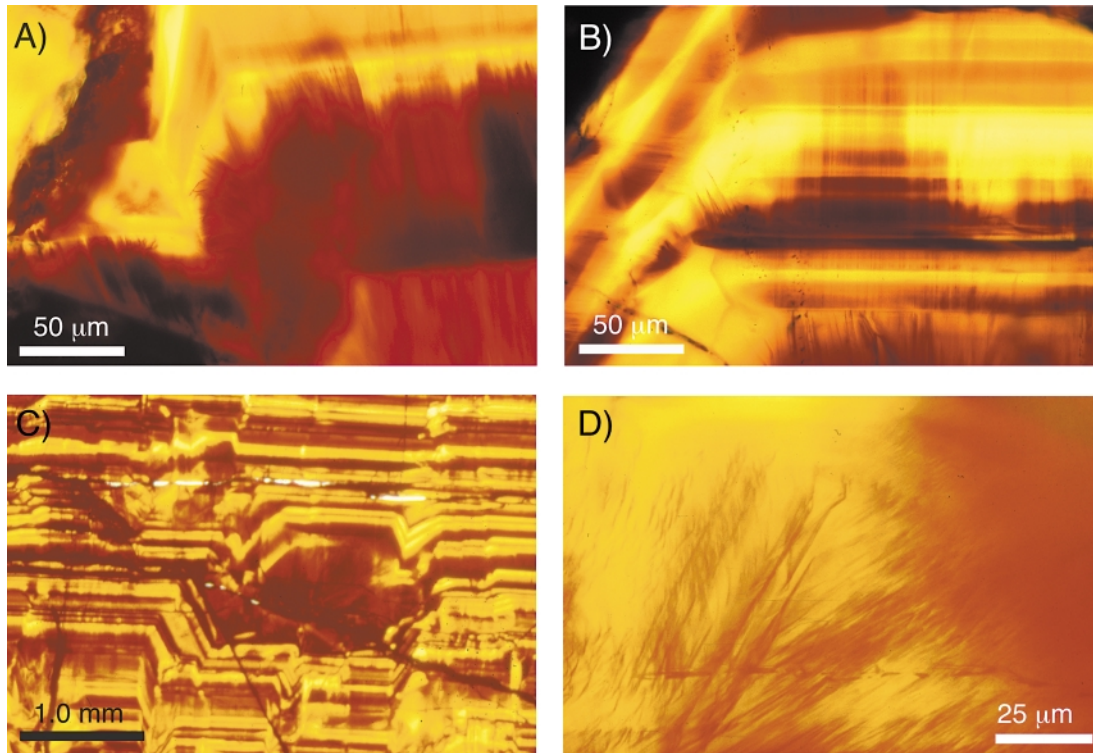


Fig. 5. A) Acicular spherulite (light grey) grows perpendicular to crystal faces from the base of a layer. B) Acicular crystals continuous across several layers of matrix spherulite display vertical oscillatory zoning. C) A trough in spherulite layering contains an arborescent aggregate of branching acicular crystals of spherulite overlain by layered spherulite moulding the arborescent aggregate. D) Detail of delicate branching acicular spherulite within the arborescent aggregate.

tions. Acicular spherulite observed under high-contrast conditions appears brighter than the matrix spherulite, thus indicating a higher mean atomic mass (Fig. 4). The elemental maps show that the dark and light brown layers are formed of Fe-rich and Fe-poor spherulite, respectively (Fig. 7A). A representative profile 0.56 mm long, perpendicular to layering, and composed of 113 analytical points evenly spaced every 5 µm, was performed at McGill University. Because the points are evenly spaced, some fall at or near layer boundaries. The profile, however, has the advantage of offering a systematic sampling of spherulite compositions. The profile reveals a bimodal distribution of Fe contents in the spherulite (Fig. 8A). Light brown spherulite has a mode near 3.25% Fe, whereas dark brown spherulite is characterized by a mode near 4.75% Fe. Substitution of Fe for Zn is demonstrated by a significant correlation coefficient, 0.938 (Fig. 8B).

The areas in which acicular spherulite is abundant are not apparent on the 1 mm × 1 mm Fe X-ray maps (Fig. 7A). X-ray maps for Ag, Sb, and Cu, however, show irregular bands enriched in these elements at the

base of some of the Fe-rich layers (Figs. 7B, C, D). These bands correspond to areas dominated by acicular crystals of spherulite, as verified optically and using back-scattered electron mapping. The Cu X-ray map (Fig. 7D) shows that Cu is also enriched within several of the Fe-rich layers; the distribution of Cu defines Cu-enriched sublayers that are thinner and at the base of the Fe-rich layer (Figs. 7A, D).

The X-ray maps for Ag, Sb, Cu and Zn display well the acicular spherulite (Fig. 9). No variation in signal is apparent on the Fe X-ray map, which suggests that in the area investigated at least, the matrix spherulite has the same Fe content as the acicular spherulite. The Zn X-ray map indicates that acicular spherulite is depleted in Zn compared to the matrix spherulite (Fig. 9D). This spatially coincident depletion in Zn and enrichment in Ag, Sb, and Cu (Figs. 9A, B, C), coupled with lack of variation of Fe, are strong evidence for substitution of Ag, Sb, and Cu for Zn in the acicular spherulite. Because of the small width of the acicular crystals, it is technically not possible to measure the composition quantitatively because the volume excited by the elec-

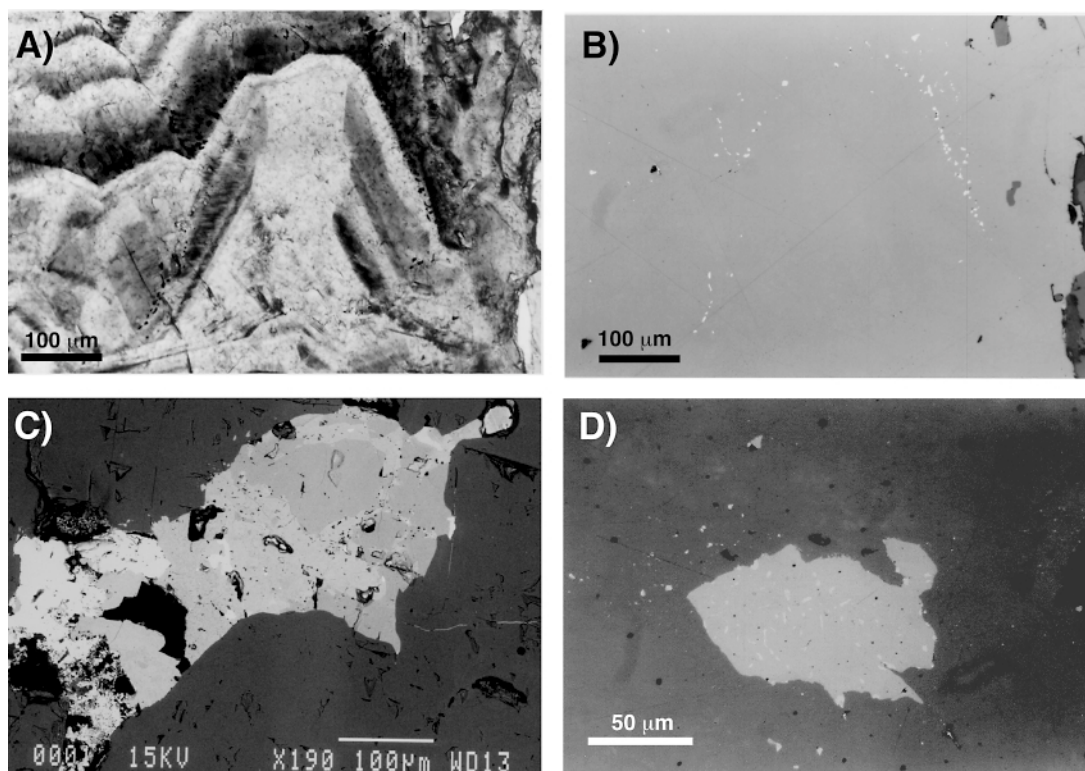


FIG. 6. A) Dark layer outlining the face of a sphalerite crystal in transmitted light. B) Reflected-light photograph of the area shown in A. The base of the dark layer is marked by a chain of complex inclusions of chalcopyrite, galena, pyrrargyrite and freibergite. C) Complex inclusion of Ag-poor freibergite (darker grey), Ag-rich freibergite (medium grey) and pyrrargyrite (light grey). D) Freibergite inclusion (light grey) in sphalerite (dark grey) with oriented or rounded chalcopyrite exsolution-induced blebs (white).

tron beam is larger than the width of the acicular crystals. Across the profile described above, the maximum concentrations of minor elements in sphalerite were 0.96 wt.% Ag, 0.55 wt.% Sb, and ~0.5 wt.% Cu. These concentrations could represent an approximation of the composition of the acicular sphalerite.

#### *Analysis of layer thickness*

The oscillatory banding has the appearance expected of a random process. To detect the presence of an underlying factor controlling the deposition of the sphalerite layers and acicular crystals, layer thickness was measured across segments of sphalerite crystals (*e.g.*, Fowler & L'Heureux 1996). A color composite photomicrograph of part of a crystal was used to measure the thickness perpendicular to the sphalerite layers along a reference line positioned arbitrarily to avoid irregularities in the layering.

A representative example is described below in which 412 thicknesses of layers were measured over a length of 4.47 mm with a precision of 2  $\mu\text{m}$ . The layers range in thickness from optical resolution to 147  $\mu\text{m}$ , and thicknesses display a log-normal distribution (Fig. 10A). The layer-thickness succession displays a complicated pattern without obvious structure (Fig. 10B). The return map of layer thickness (Fig. 10C), however, displays a clustering near the origin, with two arrays of data points plotting along the axes. A typical sequence of thicker layers displays a cycle wherein a point along the abscissa is followed by a point along the ordinate and then by points near the origin (Fig. 10C), such that a thick layer is overlain by a second thicker layer which, itself, is overlain one or several thin layers. The pattern shown in Figure 10C is similar to those reported for sphalerite from the Pine Point deposit by Fowler & L'Heureux (1996).

Figure 10D is a difference map displaying the difference in layer thickness of adjoining layers. The dif-

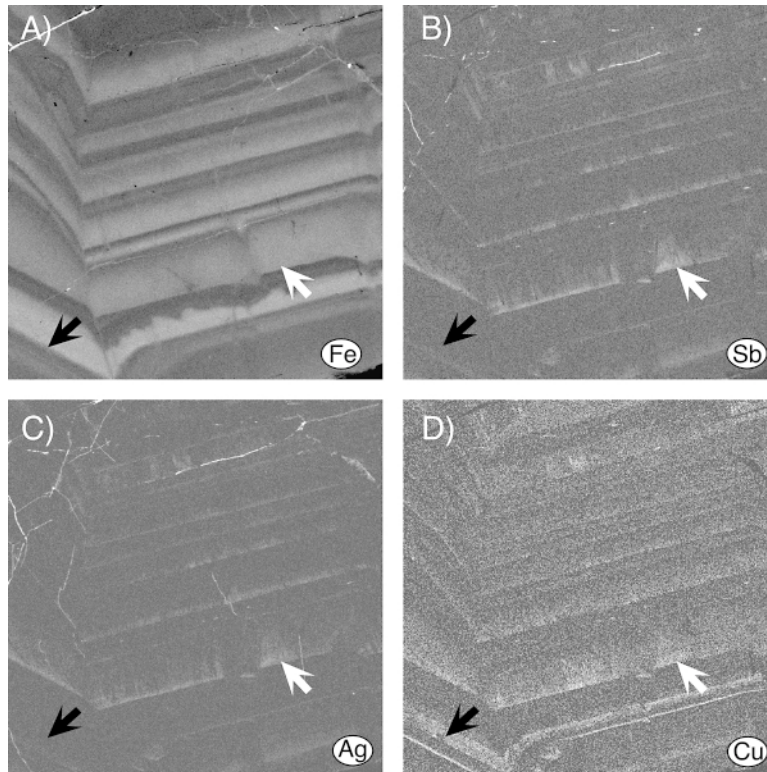


FIG. 7. Electron microprobe X-ray maps of banded sphalerite. Each map is 1 mm across, containing  $500 \times 500$  pixels. The black arrow shows massive, textureless bands with a base rich in Cu within a broader zone of Fe-rich sphalerite and a Fe- and Cu-poor top. The white arrow shows the location of acicular sphalerite depicted in Figure 8 and that is enriched in Sb, Ag and Cu but not Fe. A) Fe. B) Sb. C) Ag. D) Cu.

ference map shows a pattern in which a cluster of points near the origin is surrounded by three arrays of points: horizontal, vertical and oblique (Fig. 10D). Successive layers again show a cycle wherein several layers of similar thickness plot near the origin, because of small differences in layer thickness, and are followed by one or several cycles starting with a point toward the top along the ordinate followed by a point in the lower right corner, then followed by a point to the left along the abscissa (Fig. 9D). For some layer successions, the amplitude of the difference in layer thickness increases and then decreases from one cycle to the next until the points plot near the origin. The return map and the difference map may thus record the influence of deterministic processes controlling the succession in layer thickness (Fowler & L'Heureux 1996, L'Heureux & Fowler 1996). Layer thickness from a random population would plot as a uniform distribution of points on the return map (Fowler & L'Heureux 1996). The lognormal distribution of layer thickness in Figure 10A was reproduced using a lognormal law with a random probability and

appropriate distribution-coefficients based on the average and standard deviation of layer thicknesses measured in the sample (Fig. 10E). The modeled layer-thicknesses display a succession (Fig. 10F) not unlike that of the measured sample (Fig. 10B). The return map of the modeled thicknesses of layers (Fig. 10G) displays data points that are not randomly dispersed, but instead concentrate near the two axes, as in Figure 10C. Using this modeled layer-thickness population, the difference map (Fig. 10H) displays a pattern very similar to that of measured thickness (Fig. 10D). This simulation indicates that the layer thickness could also be a product of a random process with a lognormal distribution, and that the effect of deterministic processes is negligible in the sample studied and not detected in the layer-thickness analysis.

#### DISCUSSION

The acicular crystals of sphalerite have delicate shapes that suggest a non-turbulent hydrodynamic en-

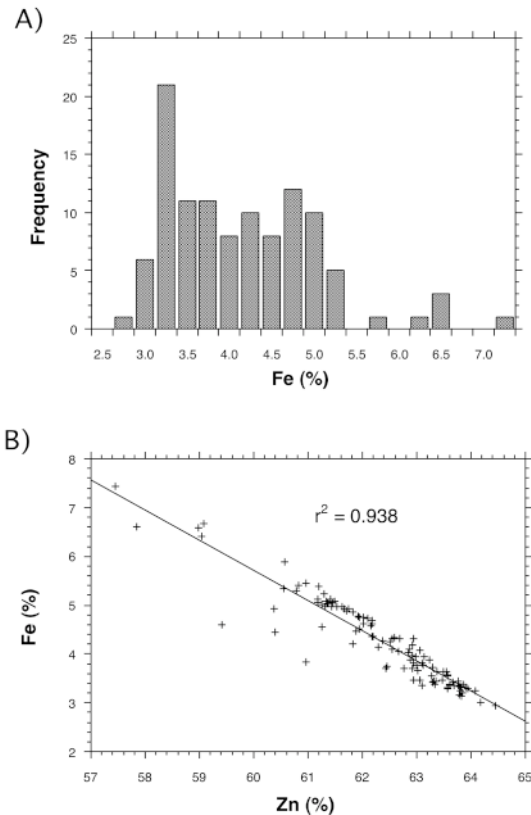


FIG. 8. A) Histogram of Fe (wt.%) in sphalerite along a profile perpendicular to sphalerite layering. Fe concentrations display a bimodal distribution, with a mode of 3.25 wt.% Fe for light-colored sphalerite, and a mode of 4.75 wt.% Fe for dark-colored sphalerite, in addition to a tail of higher Fe concentrations. B) Correlation between Fe and Zn concentrations that display Fe substitution for Zn in the structure.

vironment in the vein during growth. The direction of growth is toward the center of the veins, and the acicular sphalerite is enriched in Ag, Sb and Cu compared to the enclosing layered sphalerite that forms the upper part of layer. The base of some layers contains chains of inclusions of tetrahedrite-freibergite, pyrrargyrite, chalcocopyrite, and galena (Fig. 6) that seem to have coprecipitated with the sphalerite. The growth of acicular sphalerite seems to coincide with higher concentrations of Ag, Sb, Fe and Cu at the onset of precipitation of a layer. Growth of acicular sphalerite and sulfosalt inclusions must have progressively depleted the hydrothermal solution in Ag, Sb, Fe and Cu.

The origin of the acicular sphalerite remains enigmatic. No X-ray-diffraction evidence for wurtzite is found in the layered sphalerite. Wurtzite is known to be metastable and to invert to sphalerite with time (Scott

& Barnes 1972). Experimental data indicate that the appearance of wurtzite is favored at low temperatures by solutions enriched in cations such as Fe, Cd, Mn, Ga (Maurel 1978, Kubo *et al.* 1992, Ueno *et al.* 1996). Kojima & Ohmoto (1991) suggested that wurtzite precipitates rapidly from supersaturated hydrothermal solutions. The hexagonal symmetry of wurtzite is more likely to favor acicular crystals than is sphalerite (cubic). The acicular crystals locally branch into dendritic crystals, thus suggesting rapid precipitation. Therefore, it is more likely that the acicular sphalerite inverted from rapidly precipitated wurtzite. Dendritic wurtzite and the sulfide and sulfosalt inclusions are inferred to have precipitated from hydrothermal fluids rich in Ag-Sb-Cu-Fe, which locally became depleted in those cations. The residual fluid deposited sphalerite poor in Ag-Sb-Cu-Fe around the dendritic wurtzite. The delicate texture of dendritic wurtzite might suggest that it started to precipitate after injection of a new batch of hydrothermal fluid into a fracture, or that flow was not turbulent within the fractures, so as to preserve the acicular texture. If acicular sphalerite represents inverted wurtzite, its crystallization at the base of a layer may indicate low initial sulfur fugacity (Scott & Barnes 1972). Sulfur isotopes in vein sulfides indicate that sulfur was leached from the local country-rocks and that metals were carried by a sulfur-poor hydrothermal fluid (Beaudoin *et al.* 1992b). Acicular wurtzite might indicate transient initial low fugacity of sulfur, but the mineral assemblage does not enable one to constrain the sulfur fugacity in the veins.

Oscillatory chemical zoning in minerals can be simulated by deterministic non-linear dynamic models, such as isothermal constitutive undercooling, which consider diffusion and growth kinetics at the mineral interface with a fluid (L'Heureux & Fowler 1994, Fowler & L'Heureux 1996). The distribution of points in the return map of layer thickness (Fig. 10C) is similar to that shown for concentrically zoned sphalerite from the Pine Point Mississippi-Valley-type deposit (Fig. 6, Fowler & L'Heureux 1996) and which was interpreted to display a degree of determinism. The succession of layer thickness in the Kokanee Range sphalerite, however, can be reproduced by a random lognormal law, which suggests that the amount of crystal growth, or the layer thickness, is not controlled by deterministic but by external processes. A likely hypothesis is that the amount of fluid introduced into a fracture dictates the layer thickness that can be measured in the sphalerite crystals. Patrick *et al.* (1993) also suggested that periodic changes in pH, caused by episodic injection of hydrothermal fluids, controlled adsorption of various metal cations into zoned sphalerite. It is likely that the change in ZnS polytype and composition relates to the chemical evolution of a batch of hydrothermal fluid stored temporarily within a fracture. This process appears to operate at the scale of the ZnS layer. The layer thickness, however, displays a random lognormal distribution that is

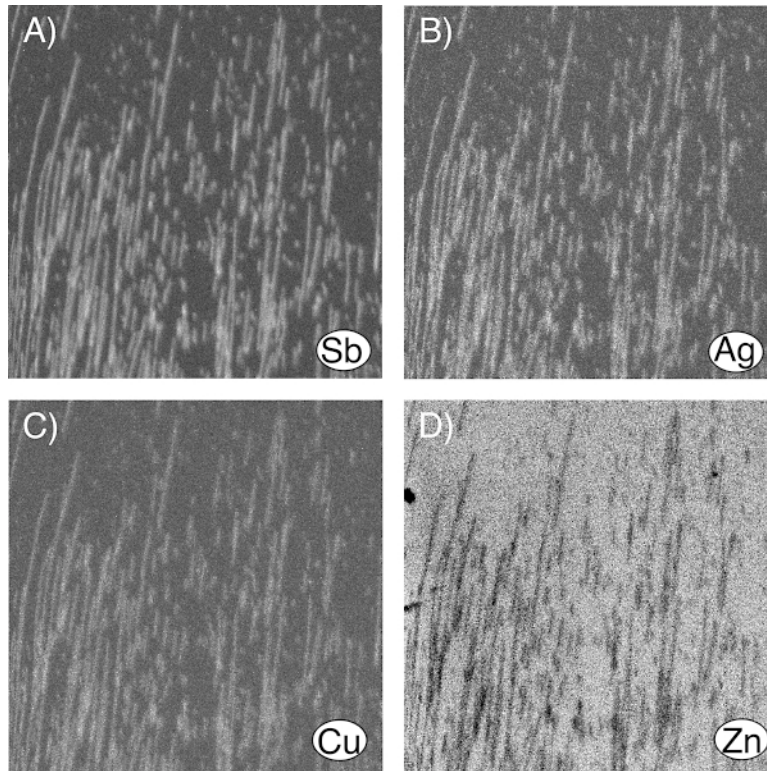


FIG. 9. Electron-microprobe wavelength-dispersion X-ray maps for the same area of acicular sphalerite. Each image is 50  $\mu\text{m}$  wide and comprised of  $512 \times 512$  pixels. A) Sb. B) Ag. C) Cu. D) Zn.

more likely attributed to injection of successive batches of hydrothermal fluid in the same open fracture.

#### CONCLUSIONS

The texture and chemical composition of acicular sphalerite suggest that it inverted from wurtzite precipitated from supersaturated hydrothermal fluids. The original wurtzite is inferred to have adsorbed Ag, Sb, Cu that substituted for Zn in the acicular crystals, whereas Cu and Fe substituted for Zn in the massive sphalerite. High concentrations of Ag, Sb and Cu in the hydrothermal fluids were progressively depleted by the inferred precipitation of acicular wurtzite to a threshold where massive embedding sphalerite precipitated. Delicate dendritic textures attest to the non-turbulent, quiescent hydrodynamic conditions during growth of the acicular crystals. The band thicknesses in sphalerite have a lognormal distribution that can be simulated by a random process; it may relate to the amount of fluid injected into the fracture. Color banding in sphalerite in the Kokanee Range appears to be controlled by processes

operating at the scale of a fracture, which precludes its use as a time marker, as in sphalerite stratigraphy.

#### ACKNOWLEDGEMENTS

Tony Fowler and Yvan L'Heureux shared many stimulating discussions on oscillatory zoning in sphalerite. Reviews by R. Hébert, Tony Fowler, D.J. Kontak and an anonymous reviewer on earlier versions of this paper are greatly appreciated. This research was funded by the Natural Sciences and Engineering Research Council.

#### REFERENCES

- BARTON, P.B., JR. & BETHKE, P.M. (1987): Chalcopyrite disease in sphalerite: pathology and epidemiology. *Am. Mineral.* **72**, 451-467.
- \_\_\_\_\_, \_\_\_\_\_ & ROEDDER, E. (1977): Environment of ore deposition in the Creede mining district, San Juan Mountains, Colorado. III. Progress toward interpretation of the chemistry of the ore-forming fluid for the OH vein. *Econ. Geol.* **72**, 1-24.

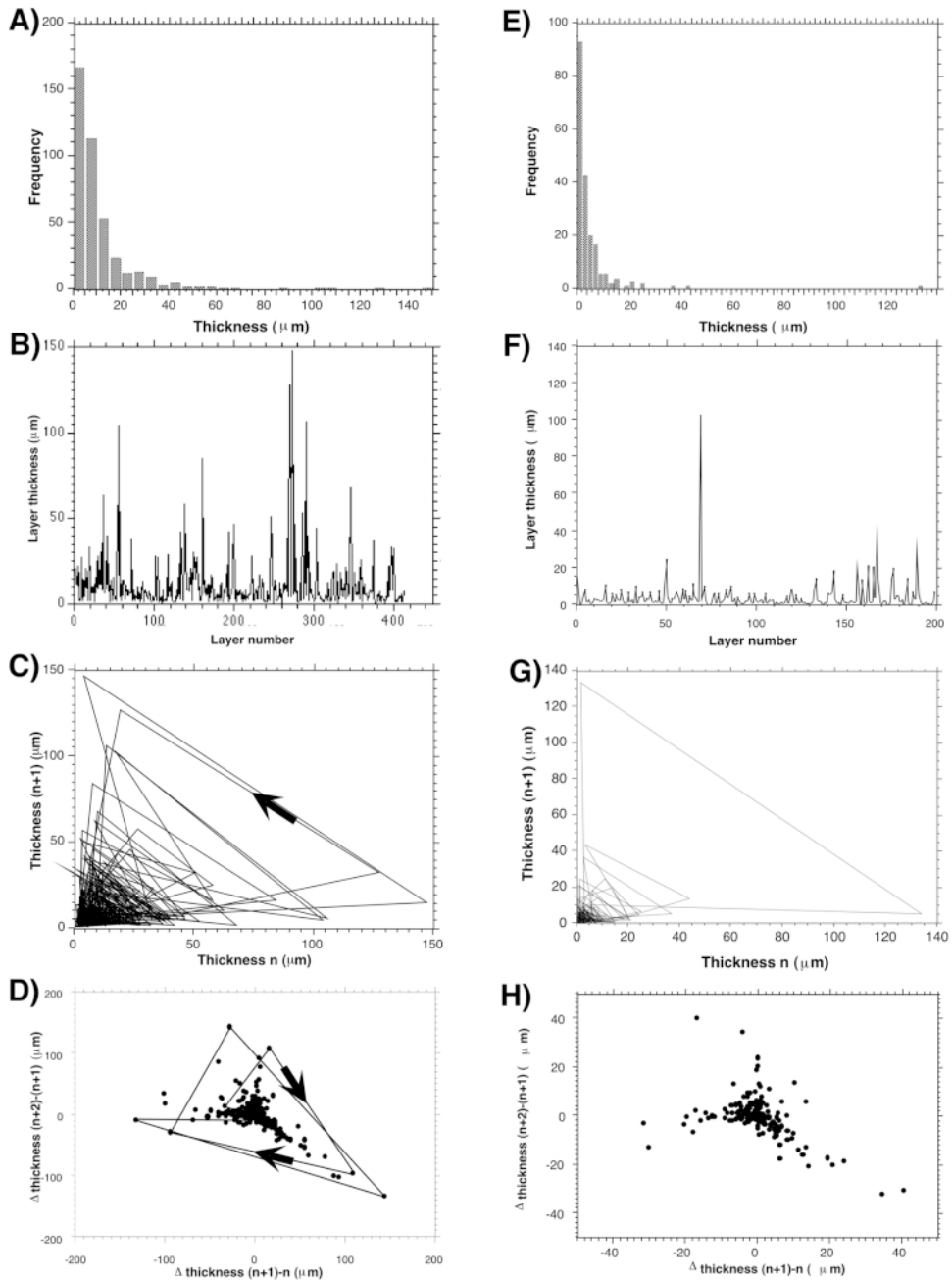


FIG. 10. A) Histogram of layer thickness in a layered sphalerite sample with an average layer-thickness of  $10.8 \mu\text{m}$  and a standard deviation of  $15.8 \mu\text{m}$ . B) Sequence of layer thickness in layered sphalerite. C) Return map comparing the thickness of a layer to that of the subsequent layer. Successive layers are joined by a line. The arrow displays the layer sequence in the direction of crystal growth. D) Difference map displaying the difference in thickness between three adjoining layers. The arrows display the typical sequence of layer differences in the direction of crystal growth. E) Lognormal distribution of random thickness of layers simulated according to a random probability using a lognormal law with a population thickness average of  $10 \mu\text{m}$  and a standard deviation of  $15 \mu\text{m}$ . F) Succession in layer thickness for the modeled random lognormal population. G) Return map of layer thickness for the modeled random lognormal population. H) Difference map of layer thickness for the modeled random lognormal population.

- BEAUDOIN, G. (1991): *The Silver-Lead-Zinc Veins of the Kokanee Range, British Columbia*. Ph.D. thesis, Univ. of Ottawa, Ottawa, Ontario.
- \_\_\_\_\_, RODDICK, J.C. & SANGSTER, D.F. (1992a): Eocene age for Ag-Pb-Zn-Au vein and replacement deposits of the Kokanee Range, southeastern British Columbia. *Can. J. Earth Sci.* **29**, 3-14.
- \_\_\_\_\_, TAYLOR, B.E. & SANGSTER, D.F. (1992b): Silver-lead-zinc veins and crustal hydrology during Eocene extension, southeastern British Columbia, Canada. *Geochim. Cosmochim. Acta* **56**, 3513-3529.
- BURKE, E.A.J. & KIEFT, C. (1980): Roquesite and Cu-In-bearing sphalerite from Långban, Bergslagen, Sweden. *Can. Mineral.* **18**, 361-363.
- DINI, A., BENVENUTI, M., LATTANZI, P. & TANELLI, G. (1995): Mineral assemblages in the Hg-Zn-(Fe)-S system at Levigliani, Tuscany, Italy. *Eur. J. Mineral.* **7**, 417-427.
- FOWLER, A.D. & L'HEUREUX, I. (1996): Self-organized banded sphalerite and branching galena in the Pine Point ore deposit, Northwest Territories. *Can. Mineral.* **34**, 1211-1222.
- JOHAN, Z. (1988): Indium and germanium in the structure of sphalerite: an example of coupled substitution with copper. *Mineral. Petrol.* **39**, 211-229.
- KOJIMA, S. & OHMOTO, H. (1991): Hydrothermal synthesis of wurtzite and sphalerite at T = 350° - 250°C. *Mining Geol.* **41**, 313-327.
- \_\_\_\_\_, & SUGAKI, A. (1985): Phase relations in the Cu-Fe-Zn-S system between 500° and 300°C under hydrothermal conditions. *Econ. Geol.* **80**, 158-171.
- KUBO, T., NAKATO, T. & UCHIDA, E. (1992): An experimental study on partitioning of Zn, Fe, Mn and Cd between sphalerite and aqueous chloride solution. *Mining Geol.* **42**, 301-309.
- KUHLEMANN, J. & ZEEH, S. (1995): Sphalerite stratigraphy and trace element composition of east Alpine Pb-Zn deposits (Drau Range, Austria-Slovenia). *Econ. Geol.* **90**, 2073-2080.
- L'HEUREUX, I. & FOWLER, A.D. (1994): A nonlinear dynamic model of oscillatory zoning in plagioclase. *Am. Mineral.* **79**, 885-891.
- \_\_\_\_\_, & \_\_\_\_\_ (1996): Isothermal constitutive undercooling as a model for oscillatory zoning in plagioclase. *Can. Mineral.* **34**, 1137-1147.
- MAUREL, C. (1978): Stabilité de la blende dans le système Zn-Cd-S. *Bull. Minéral.* **101**, 406-411.
- MCLIMANS, R.K., BARNES, H.L. & OHMOTO, H. (1980): Sphalerite stratigraphy of the Upper Mississippi Valley zinc-lead district, southwest Wisconsin. *Econ. Geol.* **75**, 351-361.
- MÖLLER, P. (1985): Development and application of the Ga/Ge-geothermometer for sphalerite from sediment-hosted deposits. *Gebrüder Borntraeger Monograph Series on Mineral Deposits* **25**, 15-30.
- OEN, I.S., KAGER, P. & KIEFT, C. (1980): Oscillatory zoning of a discontinuous solid-solution series: sphalerite-stannite. *Am. Mineral.* **65**, 1220-1232.
- PATRICK, R.A.D., DORLING, M. & POLYA, D.A. (1993): TEM study of indium- and copper-bearing growth-banded sphalerite. *Can. Mineral.* **31**, 105-117.
- RAMDOHR, P. (1969): *The Ore Minerals and their Intergrowths*. Pergamon Press, Oxford, U.K.
- SCOTT, S.D. & BARNES, H.L. (1972): Sphalerite-wurtzite equilibria and stoichiometry. *Geochim. Cosmochim. Acta* **36**, 1275-1295.
- UENO, T., SCOTT, S.D. & KOJIMA, S. (1996): Inversion between sphalerite- and wurtzite-type structures in the system Zn-Fe-Ga-S. *Can. Mineral.* **34**, 949-958.
- VIETS, J.G., HOPKINS, R.T. & MILLER, B.M. (1992): Variations in minor and trace metals in sphalerite from Mississippi Valley-type deposits of the Ozark region: genetic implications. *Econ. Geol.* **87**, 1897-1905.
- WARREN, H.V. & THOMPSON, R.M. (1945): Sphalerites from western Canada. *Econ. Geol.* **40**, 309-335.

Received November 19, 1999, revised manuscript accepted November 12, 2000.